



FINITE ELEMENT STRESS AND DEFLECTION ANALYSIS

OF CDF YOKE AND END PLUG

R. Wands, J. Grimson, R. Kephart, D. Theriot

Introduction

A large detector is being designed to study $\bar{p}p$ collisions at center-of-mass energies of up to 2000 GeV as part of the Fermilab Collider Detector Facility (CDF). The "central detector" of this facility consists of a solenoid, calorimeter yoke, and a variety of particle measurement devices.

The yoke will be a large steel structure that will provide the magnetic flux return path as well as support structure for calorimetry and other instrumentation. It must resist both electromagnetic and gravitational loads while exhibiting only small elastic deformations. The instrumented endplugs of the yoke are subjected to large electromagnetic loads. Moreover, due to the presence of wire chambers within these plugs, they must also be particularly stiff. The purpose of this paper is to present the results of a finite element stress and deflection analysis of these structures under various anticipated load conditions. The PATRAN-G finite element modeling program¹, installed on a CDF-VAX 11/780 and operating from a Ramtek 6212 colorgraphics terminal, was used to generate the analysis models. The actual finite element analysis was performed by the ANSYS general purpose finite element program², installed on the Fermilab Cyber 175's.

I. The CDF Yoke

A. The Structure

The CDF yoke is required to perform under two distinct circumstances. During detector operation in the collider area, it must provide a rigid support for the endplugs, endwall hadron calorimetry, "Roman Arch" hadron calorimetry, and solenoid.

Between experimental periods, the "central detector" consisting of the yoke, solenoid, calorimetry, and other instrumentation (totalling approximately 2400 tons) will be raised as a unit and moved to and from a nearby assembly hall.

Fig. 1 shows the yoke design as it was analyzed. It consists of two rectangular frame walls spanned by four flux return legs. The 3 ft. deep square steel frame is constructed of 8 in. thick carbon steel plate. A 2 in. thick stainless steel plate with a large circular cutout is welded to the frame. An annular ring of 2 in. thick carbon steel plate is welded at the cutout to provide a better flux path to the solenoid. A carbon steel ring composed of twenty-four 8 in. thick steel plate segments and 126 in. in radius lies inside the frame, welded about its circumference to the stainless plate. Twelve 2 in. thick carbon steel ribs project radially inward from the ring to provide support against endplug axial magnetic load. The volume between the frame and ring is filled with three layers of 8 in. carbon steel plate inserts. Current plans call for electrosag welding of inserts, ring segments and frame, providing a virtually continuous structure. The flux return legs

are 2 ft. thick and 112 in. wide, and are built of 8 in. carbon steel plate, bolted and welded along top and bottom. The legs bolt to large carbon steel blocks, which are themselves bolted to the frame. Overall yoke length is 276 in. During detector operation, the yoke will rest on four steel feet, constructed as cubes 2 ft. on a side and lying directly under the frame. During transportation to and from the assembly hall, the yoke will be hydraulically lifted on eight steel feet, each equipped with multiton rollers rolling on a steel surfaced concrete track.

In addition to the electromagnetic and gravitational loads, another area of concern is the presence of thermal stresses in the plain carbon steel/stainless steel interfaces. These could result from temperature excursions above or below the temperature at which the metals were joined. For the purposes of this analysis, it was assumed that a 40°F uniform temperature differential could occur.

The loading types, magnitudes, and locations are summarized in Table I. For the purposes of this analysis, the endplug weight (approximately 100 tons each) was neglected. Current plans call for supporting this weight with beams attached to the vertical frame members. This will produce only a small increase in the direct stress on these members. The coil weight, which is supported by the annular carbon steel ring, is negligible compared to the weight of the endwall hadron modules, supported in part by this plate, and thus has been ignored.

Table II summarizes the materials used in yoke construction and their properties.

B. The Finite Element Models

The two models used in this analysis are shown in Fig. 2 and Fig. 3. These models differ only in the feet used for yoke support. Due to geometric and load symmetry, only one-quarter of the structure was modeled. The frame, ring, return legs, and feet were modeled with eight node hex elements (ANSYS STIF45). This is an incompatible element with extra shape functions which allow the element to assume a parabolic deformation. Three elements through the thickness of frame and ring were chosen both as a modeling convenience and to accurately represent bending in these components.

The stainless backing plate, ribs, main diagonals, and inserts were modeled with four node plate elements (ANSYS STIF63). This element allows a cubic out of plane deformation, and, with incompatible shape functions, a parabolic in-plane deformation.

The difference in order of displacement fields can result in incompatibilities between plates and solids when the two are used in the same model. Also, rotational degrees of freedom are not associated with the three-dimensional solid elements (since no plate or beam type bending strain energy approximations are used in the stiffness formulation). This results in no transfer of

moments at nodes common to plates and solids and can lead to rigid body motions³. The assembly of the plates and solids in the yoke models was accomplished by creating enough common nodes to assure that no rigid body plate motion could occur. All plate/solid junctions remain incompatible, and stresses in these areas are not of great accuracy. Gross structural stiffness should be well represented, given the relatively fine grid, large difference in plate thickness and solid dimensions, and the application of loads far from the incompatibilities.

In the actual yoke, three 8 in. plate inserts will be used to partially fill the volume between the ring and frame. Due to considerations of maximum problem size and in an effort to introduce conservatism, only two 8 in. plate inserts were included in the model. The attachment of these insert elements to the ring and frame was such that no moments could be transmitted between the solids and plates. This should underestimate the stiffening effect of the inserts.

In modeling the feet used during transportation, it was assumed that the feet were only attached to the frame at the bottom horizontal frame member. No attachment to the steel block or vertical frame member was assumed.

In generating these models, all sections which will be bolted in the actual structure were assumed to be continuous. The result was a model which was stiffer than the actual structure under most types of loading. This behavior is of the greatest concern in the area of the return legs. For this

reason, a fairly fine grid was applied at these locations to obtain nodal force information which was used to estimate the behavior of the actual joint.

Fig. 4 shows the constraints used to enforce symmetry. Fig. 5 shows the magnitude and location of the loadings. The weight loading was simulated by specifying the appropriate material mass densities and applying a coordinate acceleration in the global y direction. The axial magnetic loading, which results from the reaction of the endplug to the magnetic field, was applied at the innermost node of each rib, where the endplug reaction will be taken out. The endwall hadron calorimetry module weight was applied as concentrated forces on the outer surface of the segmented ring and the innermost circumferences of the carbon steel plate. The "Roman Arch" hadron calorimetry loading was applied as concentrated forces on the lower legs, at nodal locations nearest to where the pads of the actual arches will rest. Table III summarizes some of the finite element model statistics.

The failure criterion by which the results of this analysis were evaluated was the Von Mises effective stress⁴. This is a distortion energy theory which has been shown to be accurate for ductile materials. A maximum effective stress of 10,000 psi will be tolerated for the plain carbon regions of the structure, and a maximum of 15,000 psi will be tolerated for the stainless steel plate.

C. Results

The deflected shapes under the four loadings that occur during standard operation are shown in Fig. 6. The combined effect is shown in Fig. 7. The deflection due to axial loading dominates other loading effects. Total axial deflection is .11 in. under the combined loading, of which .10 in. is due to the axial electromagnetic load. This figure is lower than the actual case, since the leg/frame interface in the actual yoke will be bolted, and not continuous as modeled. To estimate the effect of bolting, consider the model of Fig. 8.

When the bolts are properly preloaded, some material at the interface is compressed. This preload effect changes the effective stiffness of the joint. Assuming fourteen 3.5 in. diameter bolts on one side of the neutral axis, the stiffness of this joint relative to bending can be estimated by considering the axial stiffness of the bolts and preloaded material,

$$K_j = K_b + K_m$$

where K_j = axial stiffness of one row of bolts and preloaded material

K_b = stiffness of one row of bolts

K_m = stiffness of preloaded material.

For the bolts,

$$K_b = \frac{A_b E}{\ell} \quad (14)$$

where A_b = area of bolt

E = elastic modulus = 30×10^6 lbs/in.²

ℓ = length of bolt.

The stiffness of the preloaded material can be taken as the stiffness of a hollow cylinder with an inside diameter equal to the bolt diameter and an outside diameter equal to three times the bolt diameter⁵. This results in:

$$K_m = 8K_b$$

Then

$$K_b + \frac{8.33(30) \times 10^6(14)}{16.5} = 2.12(10^8) \text{ lbs/in.}$$

$$K_m = 1.70(10^9) \text{ lbs/in.}$$

$$K_j = 1.9(10^9) \text{ lbs/in.}$$

When a moment is applied to this joint, only the bolts and material which was compressed by preloading can react in tension, while all of the interface on the other side of the neutral axis can react in compression. This is analogous to reinforced concrete beam behavior, and the concrete analogy can be used to find the neutral axis⁶. This is done by balancing the area moments of the tensile area (bolts) and compressive area. From the figure, neglecting the preloaded material,

$$A_c r_c = A_b (21 - r_c)$$

and

$$56 r_c^2 = 2450 - 116.6 r_c$$

$$r_c = 5.65$$

The distance from the steel tensile area to the neutral axis is then 15.35 in. A rotational stiffness can be defined as:

$$M = K_r \theta$$

where M = applied moment (in. lbs)

K_r = rotational stiffness (in. lbs)

θ = rotation about centroid (radians)

For this geometry, if $r = 15.35$ in.

$$K_r = 2K_j r^2 = 8.9 (10^{11}) \text{ in./lbs}$$

This applied moment M for the axial load case was found from the ANSYS nodal force results to be:

$$M = 1.57 (10^7) \text{ in. lbs.}$$

Then the rotation of the bolted joint under this applied moment is:

$$\theta = \frac{M}{K} = \frac{1.57(10^7)}{8.9(10^{11})} = .00002$$

This rotation is assumed to occur in addition to the deformation that the continuous finite element model exhibited. The maximum axial deflection occurs at a distance of 172 in. from the centroid of the return leg. The additional deflection resulting from the bolted joint is then:

$$d = 172 (.00002) = .003 \text{ in.}$$

The total axial deflection is then:

$$d_{\text{tot}} = .11 + .003 = .113 \text{ in.}$$

An additional check of this result was made by modifying the finite element model in such a way that the return legs acted as if hinged to the frame. This "worst case" model predicted axial deflections of .150 in. These results indicate that the bolting

of the return legs to the frame should have a small effect on the axial displacement.

The maximum vertical deflection predicted for the "Roman Arch" loading was .016 in. , and occurs at the midspan of the lower return leg as expected. The midspan deflection of a simply supported beam under a system of concentrated loads can be used to check the finite element results. Such a simple beam model does not allow variation of deflection across the width of the beam; however, as can be seen in Fig. 9, the return leg twists slightly due to the uneven distribution of loads. A more realistic figure against which to compare beam model results might be the average deflection across the width of the leg. This average is .013 in.

Consider the model of Fig. 10. The midspan deflection can be found by superimposing the deflection due to each load. The general expression for the deflection of a simply supported beam under concentrated loading is⁷:

$$y = y_A + \theta_A x + \frac{M_A x^2}{2EI} + \frac{R_A x^3}{6EI} + \frac{W(x-a)^3}{6EI}$$

where y_A = vertical deflection at support A = 0

θ_A = rotation at support A

M_A = moment at support A = 0

R_A = vertical shear at support A

Letting the subscript on y represent the load producing the deflection then:

$$Y_{\text{tot}} = 2y_1 + 2y_2 + y_3 = 2(-.00061) + 2(-.0040) + (-.0082)$$

$$Y_{\text{tot}} = -.017 \text{ in.}$$

This is larger than the average finite element deflection of .013, as would be expected with the assumption of simple supports.

The vertical return leg deflection is subject also to the influence of the bolted joint stiffness used previously. This correction can be made by finding the moment acting at the leg/frame joint as calculated by ANSYS for the "Roman Arch" loading. This moment is:

$$M = 6.14(10^6) \text{ in. lbs}$$

The additional joint rotation and increase in midspan deflection are:

$$\theta = \frac{M}{K_r} = \frac{6.14(10^6)}{8.9(10^{11})} = 6.9(10^{-6})$$

$$\Delta y = r\theta = 102(6.8(10^{-6})) = 7(10^{-4})$$

Total midspan deflection is then:

$$Y_{\text{tot}} = -7(10^{-4}) - .016 = -.0167 \text{ in.}$$

The "worst case" model allowing no moment at the leg/frame interface, was also run for the "Roman Arch" load case. The maximum vertical deflection was .025 in., indicating again that the bolting of the return legs to the frame will have a small effect on displacement.

An important consideration for the "Roman Arch" load case is the shear stress which must be absorbed by the bolts. The combined effects of normal and shear forces on the bolts can be calculated by considering again the nodal forces at the leg/frame interface. The maximum nodal shearing and normal force occur at the same location directly behind the supporting foot (as would be expected). These values are:

$$F_{\text{shear}} = 32,000 \text{ lbs}$$

$$F_{\text{normal}} = 33,500 \text{ lbs}$$

There are 30 nodes in the finite element model along the leg/frame interface. The actual structure will have 28 bolts. Scaling the forces appropriately, the maximum shear stress in a bolt can be found as⁵:

$$\tau_{\text{max}} = \left(\frac{\sigma_n^2}{2} + \tau^2 \right)^{1/2}$$

where τ_{max} = maximum shear stress in bolt

σ_n = axial stress in bolt

τ = shear stress normal to bolt axis

Then:

$$\begin{aligned} \tau_{\text{max}} &= \left(\left(\frac{35900}{2(8.33)} \right)^2 + \left(\frac{34300}{8.33} \right)^2 \right)^{1/2} \\ &= 4647 \text{ psi} \end{aligned}$$

If all 28 bolts act in parallel, this stress is within the capacity of the bolt material. However, as an added precaution, a shelf (possibly an extension of the support foot itself) will be added to relieve the shear in the bolt.

The current assembly plans call for bolting the plates of the return legs together and welding them top and bottom to a depth of about 1/2 in. This weld must resist any shear in the y-z plane. By finding the maximum values of these shearing stresses as calculated by the finite element model and assuming them to act on the entire face of an element, total shearing forces can be calculated and checked against the weld shear area. The maximum values of the appropriate shears are:

$$\tau_{xy} = 83 \text{ psi}$$

$$\tau_{xz} = 37 \text{ psi}$$

Using the element dimensions shown in Fig. 8, the resolved shearing force is:

$$\begin{aligned} F_s &= \left((83(272))^2 + (37(272))^2 \right)^{1/2} \\ &= 24717 \text{ lbs} \end{aligned}$$

Applying this force to the weld area gives the nominal shear stress in the weld:

$$\tau = \frac{24717}{2(11.34)(.5)} = 2180 \text{ psi}$$

This is within the capacity of the weld material. Moreover, this calculation is conservative since it is assumed that the two maximum shear values used act in the same element, which is not true. The combined stress effects of normal forces on the weld are not accounted for since bending stress information about the z axis was not available from the single element used through the leg thickness. Nodal force output indicates, however, that these forces are low. For example, the maximum nodal force acting in the x-direction for an element in the return leg is:

$$F_x = 17,370 \text{ lb}$$

Assuming this force acts on a weld which is as long as the length of an element and already under the above shear stress, then the maximum shear stress in the weld is:

$$\tau_{\max} = \left(\left(\frac{17370}{2(11.34).5} \right)^2 + 2180^2 \right)^{1/2}$$

$$\tau_{\max} = 2664$$

These figures indicate that the proposed return leg has adequate strength to support the Roman arches.

The weight loading and endwall calorimetry module loading are the least severe loading cases. Both deflections and stresses are small, and deflection patterns are intuitively reasonable. Table IV summarizes the deflection results for all of the operation load cases.

The maximum centroidal value of Von Mises effective stress as calculated by ANSYS for the STIF45 solid elements of the model was 4420 psi for the combined loading. This occurs in the large segmented ring and is the result of the axial load and its tendency to bend both the ring and frame.

Fig. 11 is a contour plot (lines of constant stress) of the Von Mises effective stresses in the ring and frame on a section taken 6 in, from the surface of the ring, and clearly shows the concentration of stress in the ring. The additional nonaxisymmetric loadings on the structure are responsible for this concentration appearing slightly below the horizontal centerline of the endwall.

The bending effect of the axial load is clearly seen in Fig. 12, which is a contour plot of the bending fiber stresses in the frame and return legs. The plot shows a section through the structure 4 in. from the surface of the frame and legs.

The most highly stressed plate elements occur in the ribs under combined loading. Centroidal stresses of 6300 psi were calculated by ANSYS for elements near the axial loading points. These high values are to be expected since the axial load is applied at a single node on each rib. The actual structure will transmit the axial load from the endplug to the ribs through some area contact and will produce stresses smaller than these calculated values. Fig. 13(a) shows the deformation of a typical rib, and Fig. 13(b) shows the Von Mises effective stress gradients in the middle section of the plate, illustrating the

concentration of stress at the load point. No stress values are presented on the plot because the element mesh is too coarse to produce meaningful figures with the interpolation procedure by which ANSYS computes nodal stresses.

Midplane centroidal stress results for the main diagonals indicate that they act as deep beams under the combined loading, resisting axial deformation by developing considerable shear stress. Fig. 14 shows the distortion and the centroidal values of in-plane stress (in the element coordinate system) for the diagonals.

The yoke distortion which results during support of the yoke on the eight feet by which it is to be transported is shown in Fig. 15(a). The Roman arch calorimetry has the largest effect on deformation. The maximum deflection of .035 in. occurs at the bottom return leg as indicated in the figure.

Reaction force data indicates that the total yoke and instrumentation weight applied to the model is 2153.5 tons. This figure does not include the two end plugs (100 tons apiece) or the third layer of 8 in. plate inserts which lie between frame and ring. These additional structures should result in a total yoke and instrumentation weight of 2400 T.

Fig. 15(b) indicates the reaction force seen by each foot. The endplug weight will be supported by the vertical frame members and will tend to increase the load seen by the outer foot.

Stresses in the structure during transportation are negligible. Fig. 15(c) shows the bending stresses in the leg and frame.

The finite element stresses and deflections indicate that the structure is adequately designed to withstand the static loading that occurs when the yoke is raised on its eight feet for transportation. Effects due to dynamic loads and/or load imbalances that might occur during the actual rolling procedure were not examined. However, on the basis of the static calculations, it seems likely that these problems will be manageable.

An area of concern during both operation and transportation of the central detector is the relative axial deformation of the annular carbon steel plate to which the coil is attached. The coil will be connected at the 12 locations corresponding to the ribs, and large relative movements of these locations could impose large stresses on the coil package. Fig. 16(a) shows the deformed shape of the plate under combined operational loading ("Roman Arch" central hadron calorimetry, endwall hadron calorimetry, weight, and axial magnetic loading). The maximum relative axial displacement occurring between ribs is .01 in. , and occurs between the locations indicated. Fig. 16(b) shows the deformed shape of the plate during transportation ("Roman Arch" calorimetry, endwall calorimetry, and weight). The maximum relative axial displacement between ribs is .02 in. occurring at the locations shown. It is felt that these distortions should

not have a serious effect on the integrity of the coil package in the detector if the coil mounts are designed to permit these relative motions.

In addition to these mechanical loads, stresses and deflections induced in yoke by temperature changes were also investigated.

A thermal load, applied as a uniform 40°F rise in structure temperature, produced a maximum deflection of .12 in. This occurs as a vertical displacement at the top of the structure, as indicated in Fig. 17(a). This is a result of the expansion of the vertical frame members (368 in. long) and foot (24 in. long). This can be verified by a crude calculation of thermal expansion based on these lengths.

$$\delta l = \alpha l \Delta T$$

where δl = change in length

l = initial length

ΔT = temperature differential

α = coefficient of thermal expansion

Substituting the appropriate quantities:

$$\delta l = 6.5 (10^{-6}) (368 + 24) (40)$$

$$\delta l = .102 \text{ in.}$$

The variation from the finite element answer is probably the result of the stainless plate expanding to a greater degree ($\alpha = 9.6 (10^{-6}) \text{ in./in.}^\circ\text{F}$) and, due to its attachment to the frame, increasing the expansion of this member.

Fig. 17(b) shows the nodal Von Mises effective stress contours in the region of the junction between the stainless plate and the annular plain carbon plate, at the plate mid-plane. The largest calculated stress along this interface is approximately 3000 psi.

Accurate thermal stresses in the junctions between frame and plate are not possible due to the incompatibilities of the solid/plate connection. However, due to the large thermal mass of the structure, large temperature variations caused by brief transients in ambient temperature are unlikely. Also, ductile stainless welds will be used at all connections, enabling stress redistribution in areas of high stress concentration.

The present yoke has the capability to withstand temperature variations which may be encountered during assembly or operation. However, it should be remembered that such temperature variations will change the normal center of the magnet with respect to the plan by about $1.5 \text{ mil}/^{\circ}\text{F}$.

D. Conclusions

The current yoke design has adequate strength and stiffness to withstand the electromagnetic and weight loadings expected during detector operation. Maximum axial displacement of the yoke endwall relative to the beam crossing point should not exceed .113 in. during operation, and maximum vertical displacement of the lower return leg should not exceed .05 in.

Stress encountered during operation should be well within the limits of the yoke materials.

Transportation of the central detector will impose no significant stresses or deflections on the yoke components. Attachment of the solenoid to the yoke should present no problems provided that the method of attachment allows for the .02 in. relative axial displacement occurring in the carbon steel plate during transportation. Thermal strains in the stainless steel/carbon steel interfaces resulting from temperature excursions should not be significant.

II. Endplug

A. The Structure

The endplugs consist of 2 in. thick steel plates assembled with an air space between layers to accommodate wire chambers used for hadron calorimetry. The external geometry of the non-re-entrant plates is that of a right frustrum of a cone with a vertex angle of 30° . The four re-entrant plates are of a constant diameter, about 2 in. smaller than the i.d. of the vacuum shell of the superconducting coil. The endplugs fit into the yoke endwall, and the ED/Saver beam pipe penetrates through a 10° conic hole in the plug's centers. The endplug weight is supported by beams which span the endwall vertical members. These beams also move axially to allow endplug and endwall module removal. The axial electromagnetic forces acting on the endplug are transmitted to the endwall via the 12 endwall ribs.

Fig. 19 shows the basic endplug geometry as analyzed. This consists of 20 steel plates connected along their inside radius by straps .75 in. thick and occupying 50 percent the inner circumference. The 20 plates are all 2 in. thick with the exception of plate No. 5, which is 2.5 in. thick. Support at the outer radius is provided by twelve 1.5 in. steel ribs, running axially through the plug from plate No. 5 through plate No. 20. These ribs extend radially inward from the outer circumference of each plate approximately 20 percent of the total distance between inner and outer radii. Plates No. 1 through 5 are supported along the outer circumference by straps .75 in. thick in the same manner as the inner radii supports. Current assembly plans call for welding of the plates to the ribs and inner radii straps. The outer straps on the re-entrant plates will be bolted in place.

The loading considered in this analysis was the axial magnetic force the endplug experiences during detector operation. The forces applied to each plate were calculated by Yamada⁸, and converted for the purposes of this investigation to uniform pressures over the surface of the first 13 plates. Table V summarizes the magnitude and direction of the pressure loadings. The total force acting on the endplug is $1.4(10^6)$ lbs.

Table VI summarizes the material properties of the steel plate used for the endplug.

B. The Finite Element Models

Several finite element models involving different combinations of ribs and straps in different sizes were generated, with the current design being considered the best compromise for both physics and structural purposes.

The analysis involved two steps:

1. Generation of a "crude" finite element model using the STIF63 four node quadrilateral element. This model was used to study deflection and locate regions of high stress.
2. Generation of a refined finite element model using the STIF45 8 node solid element in the regions of high stress located by the crude plate model. Boundary conditions were obtained from the nodal force output of the plate model.

The symmetry of geometry and loading allowed modeling of only a 30° segment of the plug. Rotational and displacement boundary conditions were applied at the radial cuts to enforce symmetry. The crude plug model used 40 STIF63 elements to model each segment of plate, this being nearly the maximum allowed by the central memory size of the Cybers. Two STIF63 plate elements were used in the radial direction on the rib. Fig. 19 shows the crude plug model, with boundary conditions and loadings indicated. For the purposes of this investigation, the outer edge of the rib at plate 20 was assumed to be fixed in all translational displacements. The actual nature of the connection

of the rib to the endwall will be analyzed separately, but the connection should be rigid enough to ensure no significant increase in the displacements calculated here.

Fig. 20 shows the refined plug model. This is a refinement of the segments of plates 19 and 20 and the stiffening rib, which was indicated by the crude model to be the region of highest stress. Eight STIF45 solid elements were used in the radial direction on the rib and, to simplify the input of boundary conditions and reduce problem size, plate elements were used in the noncritical portions of the plates. The nodal forces computed by the crude model for the boundary (rib and straps) were input as external forces at the appropriate nodes, and translational and rotational displacement constraints were applied to enforce symmetry.

Table VII summarizes some of the finite element model statistics for this analysis.

C. Results

1. "Crude" Plate Model

Fig. 21 shows the distorted geometries of plate No. 7, where the maximum axial (x) deflection of .038 in. occurred. The deflections for the model indicate that the axial movement at the inner radius of the plates varies by no more than 2 percent from plate to plate indicating that the strapping on the inner radius serves to couple the plate reactions.

Examination of the rib elements indicate that the ribs are resisting the load by in-plane shear, as expected. The maximum Von Mises effective stress value predicted by this model is 9000 psi and occurs in the rib between plates 19 and 20.

The spaces between the plates of the endplugs will contain wire chambers constructed such that the wires run tangent to the plates' circumference. The relative axial deformation along an arc of constant radius must, therefore, be small enough to ensure proper chamber function. Examination of the crude plate model nodal displacements shows the maximum relative axial displacement to be less than .006 in. This should cause no difficulties with the wire chambers.

2. Refined Solid Model

The refined solid model produced a maximum deflection of .034 in. The deflection predicted by the crude model at the corresponding location is .036 in., indicating good agreement in stiffness between the models.

Fig. 22 shows the Von Mises effective stresses calculated at the centroid for the 16 elements in the rib between plates 19 and 20. The maximum value is 17924 psi. This is a large increase over the maximum value from the crude model, and illustrates the large stress gradient in the rib. It should be noted, however, that no weld fillet is included in the model. The presence of a fillet in the weld area between plates and ribs will serve to limit the stress concentration in the rib.

Nodal Von Mises effective stress plots through a rib section and plate are shown in Fig. 23. Numerical values in this local high gradient region of the rib will probably be higher than shown, but should not exceed 20,000 psi. The gradients are clearly shown in the plots.

D. Check of Deflection Results

A simple check of the bending performance of the STIF63 element was performed to assess its accuracy when applied to the endplug plate geometry. Plate No. 5 was isolated as a separate structure, constrained with simple supports around the outer circumference and loaded with the appropriate pressure. Two methods of calculating the axial deflection of the plate were employed - the finite element solution, using the same grid which was used on plate No. 4 in the crude plug model, and the closed formed solution of Roark and Young. The finite element result predicts deflections of .212 in. The closed form solution calculates deflections of .211 in. These figures agree to within .5 percent. This indicates that the grid used should represent the plate bending stiffness of the endplug very well.

E. Conclusions

The total axial deflection of the endplug under the assumed electromagnetic loading should be .038 in. , not including the deflection of the structure by which plate 20 of the plug is attached to the endwall ribs. The use of twelve 1.5 in. thick

ribs will keep maximum Von Mises effective stresses at or below 20,000 psi.

References

1. PDA Engineering, 1560 Brookhollow Drive, Santa Ana, CA 92705.
2. Swanson Analysis Systems, P. O. Box 65, Houston, PA 15342.
3. Citipitioglu, E. , Nicolas, V. T., Ecer, A., "Utilization of Isoparametric Shell Elements in Solution of Practical Problems," Paper presented at Second World Congress on Finite Element Methods, Boumemouth Dorset, England, October 23-27, 1978.
4. Desai, C. S., and Abel, J. F., "Introduction to the Finite Element Method," Von Nostrand Reinhold, 1972.
5. Shigley, J. E., "Mechanical Engineering Design", Third Edition, McGraw-Hill, 1977.
6. Popov, E. P., "Mechanics of Materials", Second Edition, Prentice-Hall, 1976.
7. Roark, R. J., Young, W. C., "Formulas for Stress and Strain," Fifth Edition, Mc-Graw-Hill, 1975.
8. Yamada, R., CDF Coil Engineering Design Report 16, Fermilab Internal Report (unpublished) 1981.

Table I

Loading of Yoke Finite Element Models

(Magnitudes correspond to load on one-fourth of yoke)

| <u>Load</u> | <u>Magnitude</u> | <u>Method of Application</u> | <u>Operation</u> | <u>Transportation</u> | <u>Thermal</u> |
|--|-------------------------|------------------------------|------------------|-----------------------|----------------|
| Weight of yoke | $4(10^5)$ lbs | Coordinate acceleration | X | X | |
| Axial magnetic | $7(10^5)$ lbs | Nodal forces | X | | |
| Weight of "Roman Arch" Hadron calorimetry | $3.6(10^5)$ lbs | Nodal forces | X | X | |
| Weight of endwall Hadron calorimetry | $3.12(10^5)$ lbs | Nodal forces | X | X | |
| Thermal | $\Delta T = 40^\circ$ F | Uniform ΔT | | | X |

Table II

Yoke Material Properties

| Steel | Elastic Modulus (PSI) | Poisson's Ratio | Coefficient of Thermal Expansion (in/in ^o F) | Density (lb·sec ² /in ⁴) | Yield Strength (PSI) |
|-------|--------------------------|-----------------|---|--|-------------------------|
| 1020 | 29(10 ⁶) | .3 | 6.5(10 ⁻³) | 7.35(10 ⁻⁴) | 30(10 ³) |
| SS304 | 28(10 ⁶) | .3 | 9.6(10 ⁻³) | 7.50(10 ⁻⁴) | 30(10 ³) |

Table III

Yoke Finite Element Model Statistics

| # Solid Elements (STIF45) | # Plate Elements (STIF63) | Active Degrees of Freedom | Maximum Wave Front | Time to Triangularize Matrix |
|------------------------------|------------------------------|------------------------------|-----------------------|---------------------------------|
| 742 | 514 | 10770 | 301 | 383 cp sec |

Table IV

Maximum Deflections in Yoke Finite Element Models

| Model | Load Type | Maximum Deflection (in.) | | |
|----------------|--|--------------------------|--------------|-----------|
| | | X (Horizontal) | Y (Vertical) | Z (Axial) |
| Operation | Gravity | -.003 | -.007 | .002 |
| | Axial magnetic | .010 | -.028 | -.100 |
| | "Roman Arch" hadron calorimetry | .002 | -.016 | -.010 |
| | Endwall hadron calorimetry | -.002 | -.005 | -.001 |
| | Combined | .010 | -.045 | -.106 |
| Transportation | Combined weight, "Roman Arch" hadron calorimetry and endwall hadron calorimetry | -.006 | -.035 | -.032 |
| Thermal | Thermal | .046 | .12 | .038 |

Table V

Pressure Loading for Crude Plug Model

| Plate No. | Pressure ((-) sign is toward detector center) |
|-----------|--|
| 1 | 11.67 |
| 2 | 3.97 |
| 3 | - 2.12 |
| 4 | -12.11 |
| 5 | -31.73 |
| 6 | -24.38 |
| 7 | -21.70 |
| 8 | -19.68 |
| 9 | -11.94 |
| 10 | -11.35 |
| 11 | - 7.22 |
| 12 | - 4.64 |
| 13 | - 2.25 |

Table VI

Properties of Endplug Material

| Steel | Elastic Modulus (PSI) | Poisson's Ratio | Coefficient of Thermal Expansion (in/in ^o F) | Density (lb·sec ² /in ⁴) | Yield Strength (PSI) |
|-------|--------------------------|-----------------|---|--|-------------------------|
| 1020 | 29 (10 ⁶) | .3 | 6.5 (10 ⁻³) | 7.35 (10 ⁻⁴) | 36 (10 ³) |

Table VII

Plug Finite Element Model Statistics

| <u>Model</u> | <u># Solid Elements (STIF45)</u> | <u># Plate Elements (STIF63)</u> | <u>Active Degrees of Freedom</u> | <u>Maximum Wave Front</u> | <u>Time to Triangularize Matrix</u> |
|--------------|--------------------------------------|--------------------------------------|--------------------------------------|-------------------------------|---|
| Crude | | 884 | 6240 | 264 | 367.8 cp sec |
| Refined | 1252 | 210 | 13026 | 298 | 440.8 cp sec |

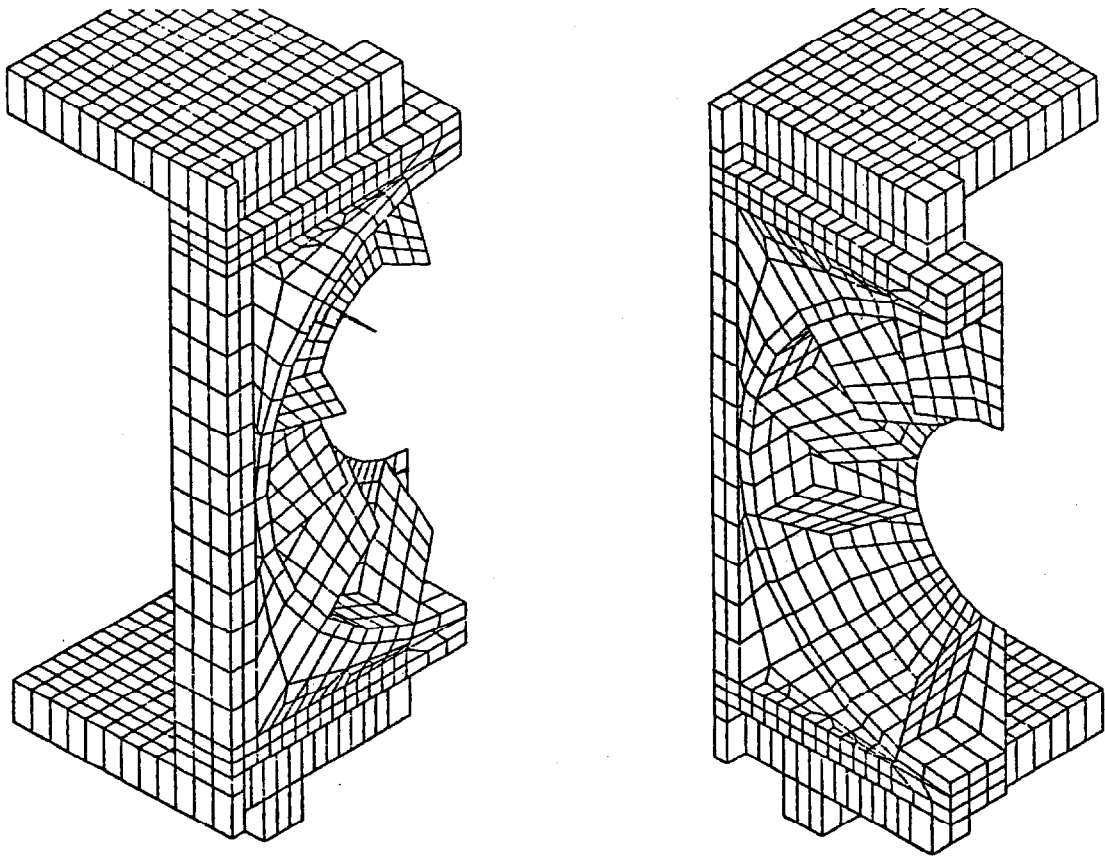


Fig. 2 Finite Element Model - Operation

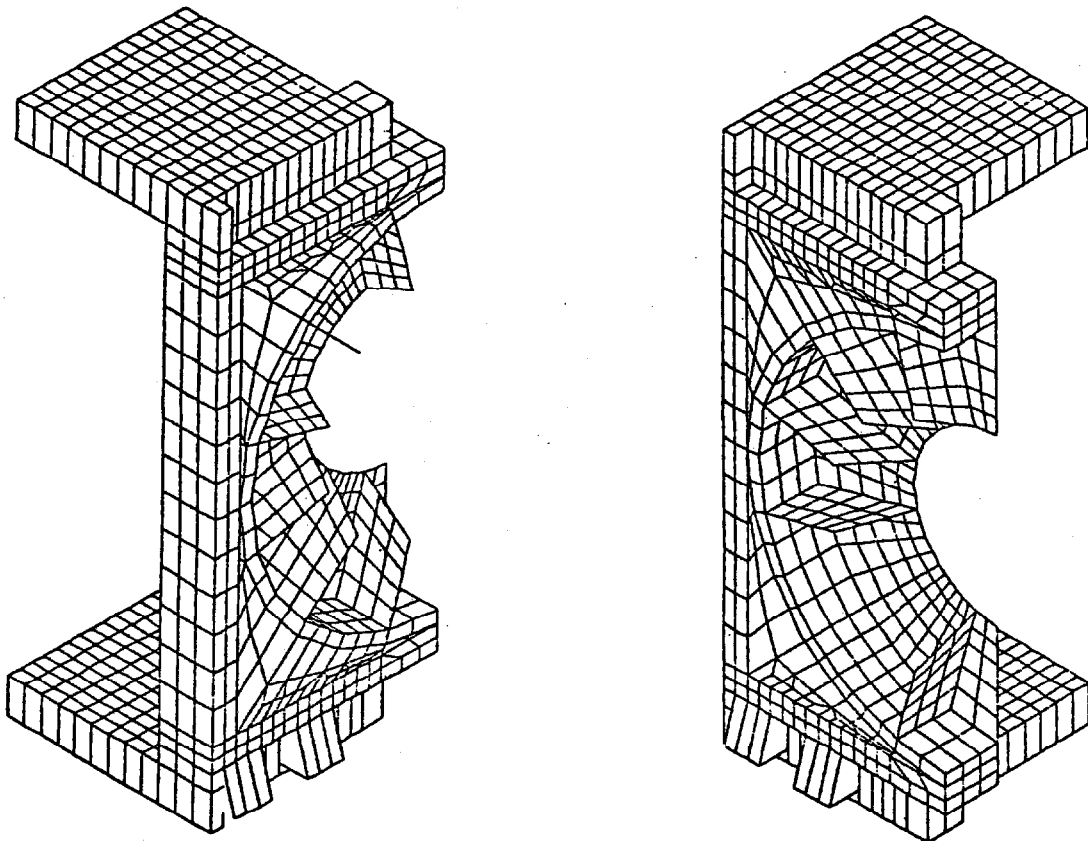


Fig. 3 Finite Element Model - Transportation

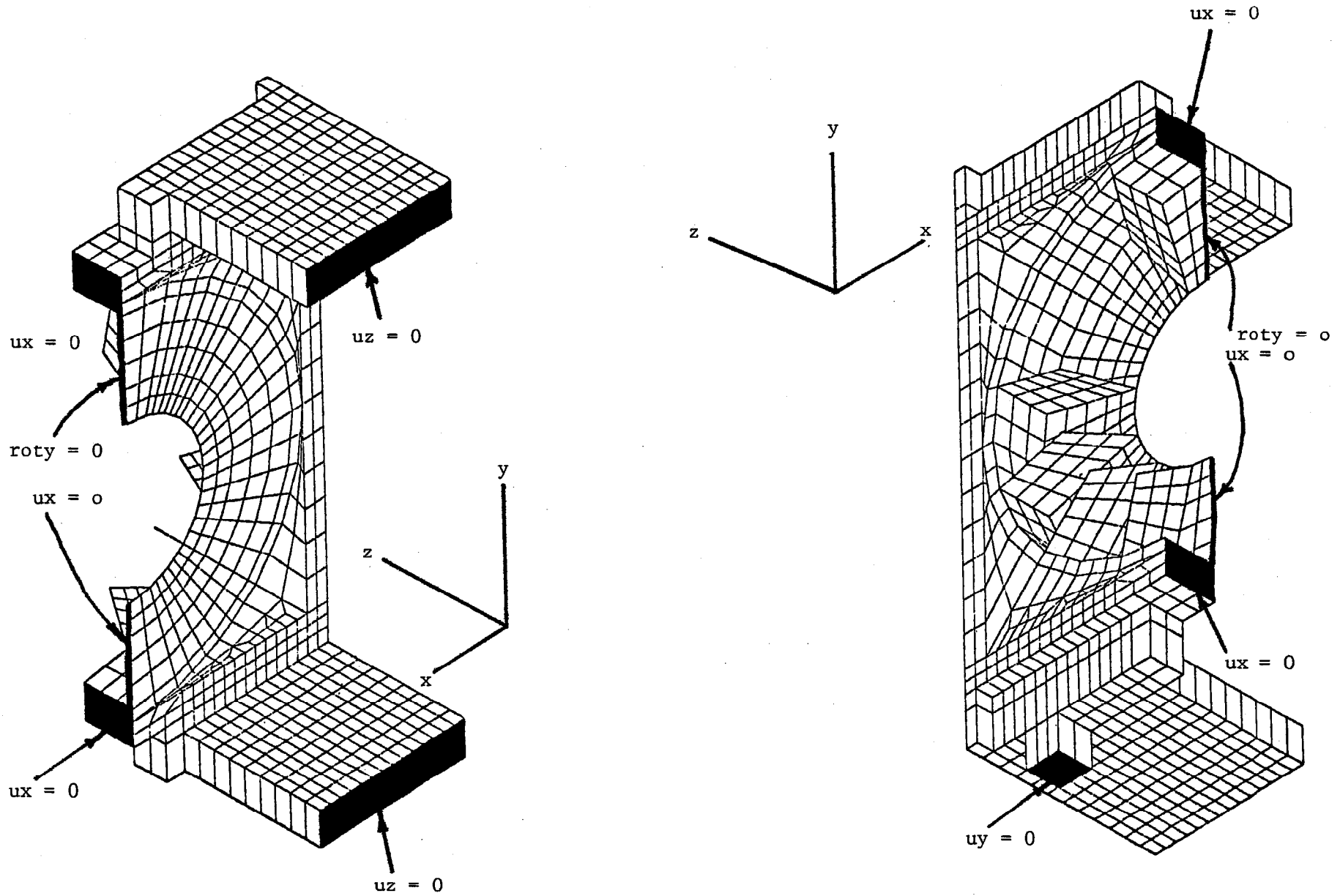
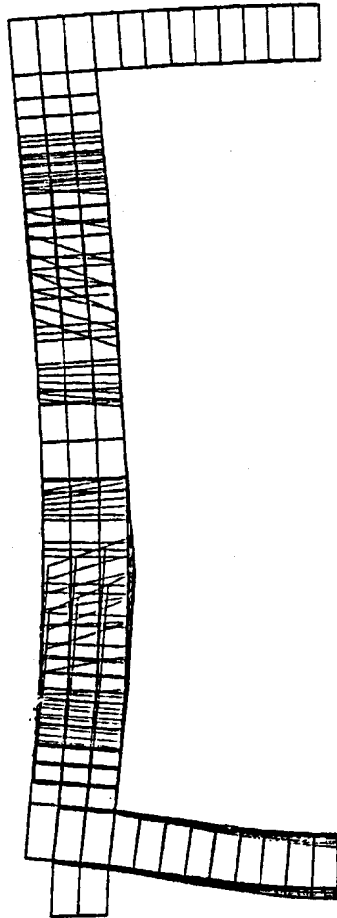


Fig. 4 Constraints applied to Yoke Finite Element Model

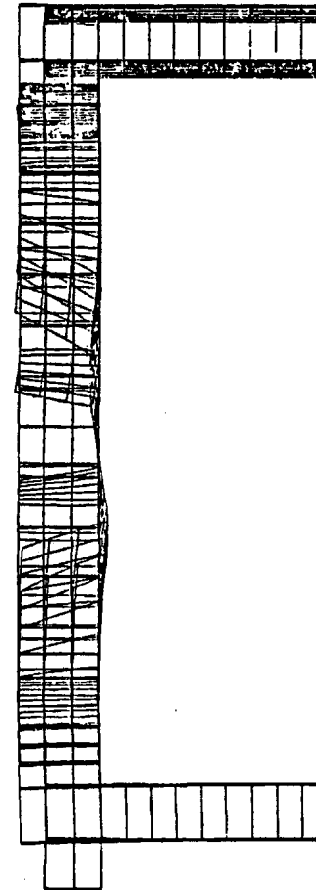
STEP 3 ITER 1 TIME .00



ROMAN ARCH LOADING

(c)

STEP 4 ITER 1 TIME .00



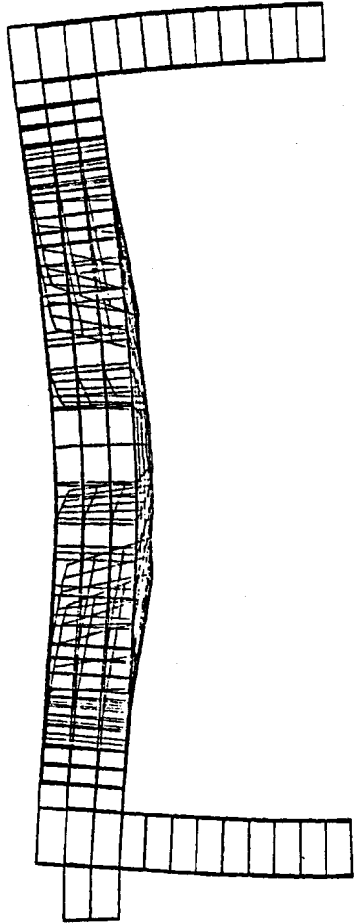
END MODULE LOADING

(d)

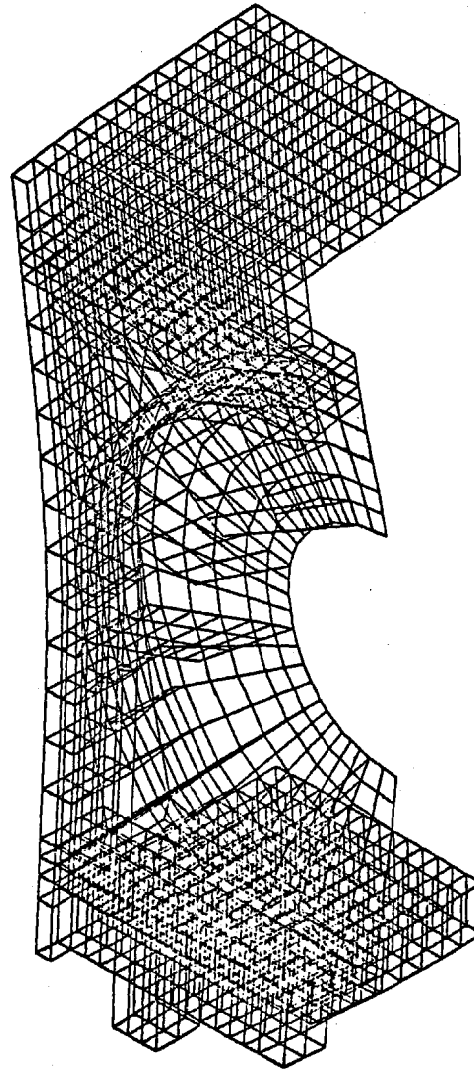
Fig. 6 Deflected Shape of Yoke Under "Roman Arch" and End Module Gravitational Loads

STEP 1 ITER 1 TIME .00

STEP 1 ITER 1 TIME .00

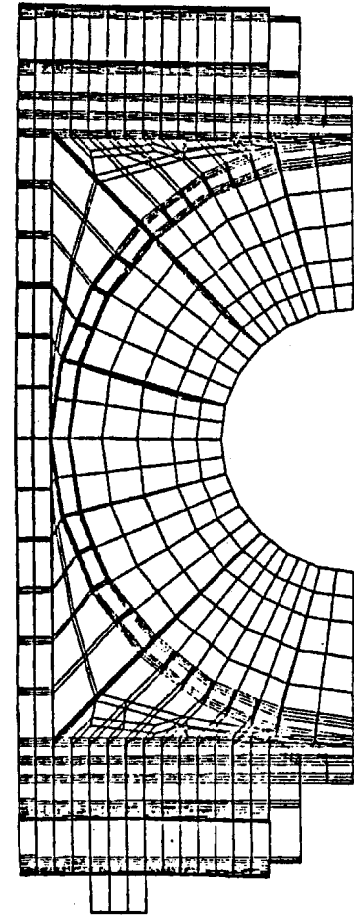


COMBINED LOADING-OPERATIONAL



COMBINED LOADING-OPERATIONAL

STEP 1 ITER 1 TIME .00



COMBINED LOADING-OPERATIONAL

Fig. 7 Deflected Shape of Yoke Under Operational Loads (All Gravitational and Magnetic Loads Applied)

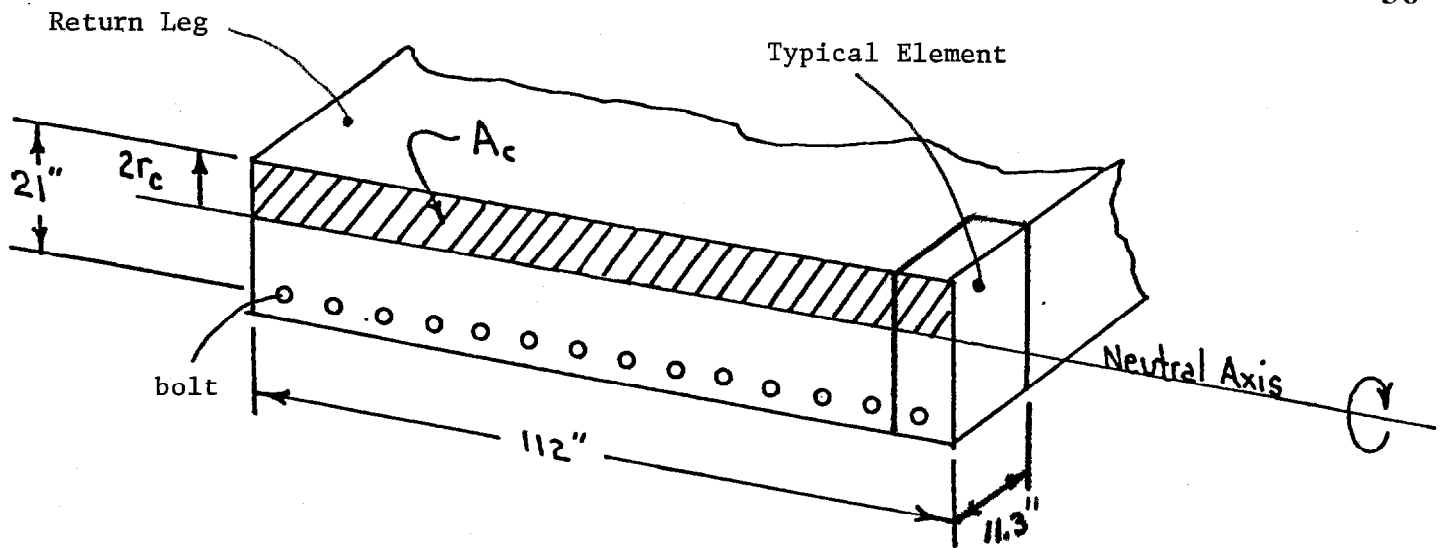
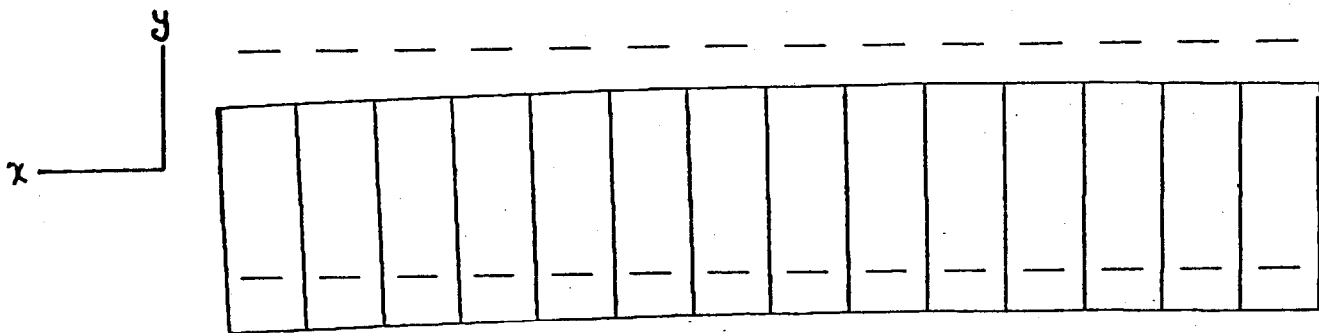


Fig. 8 Leg/Frame Interface Model for Estimating Effect of Bolted Connection



TWIST IN RETURN LEG DUE TO ROMAN ARCH LOADING

DISP ANSYS

Fig. 9

$$P_1 = 90(10^3) \text{ lbs.}$$

$$P_2 = 90(10^3) \text{ lbs.}$$

$$P_3 = 90(10^3) \text{ lbs.}$$

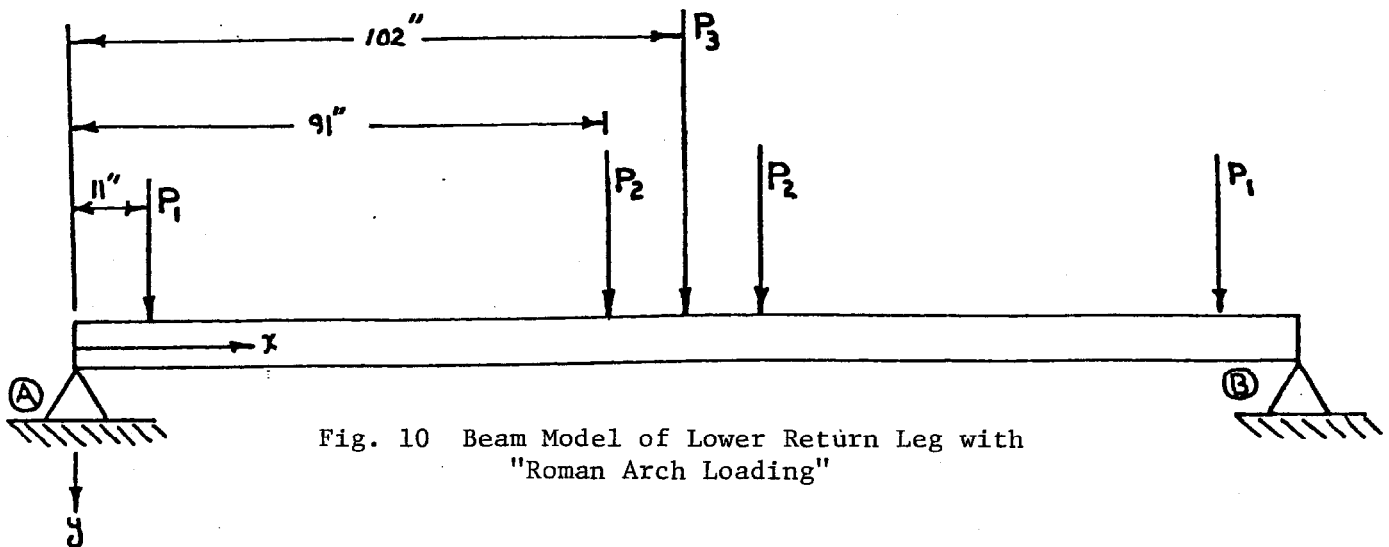
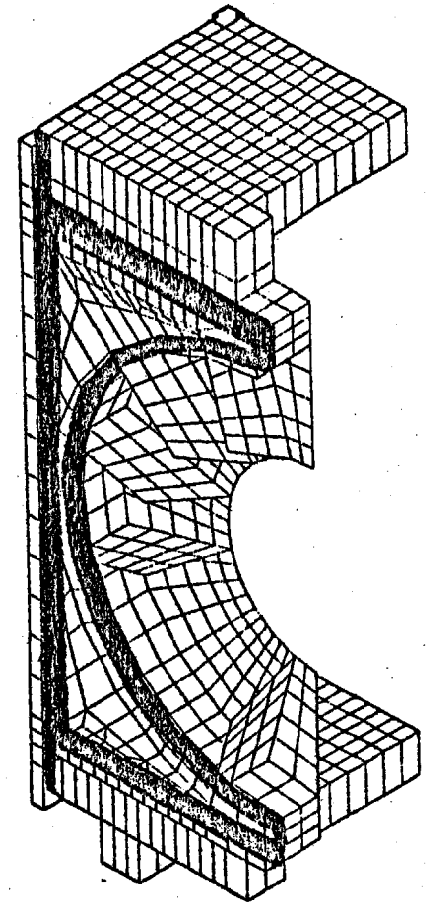
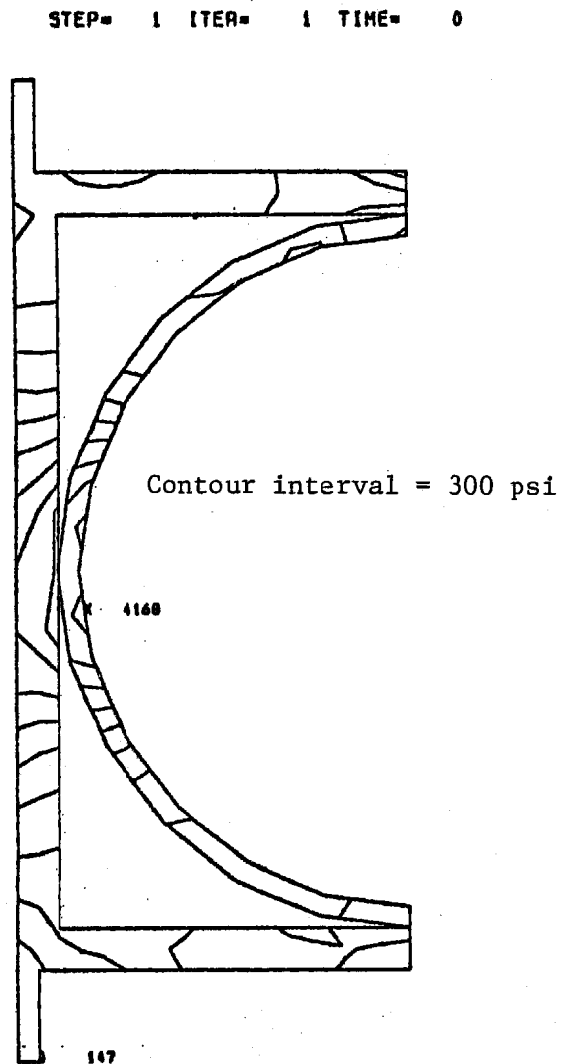


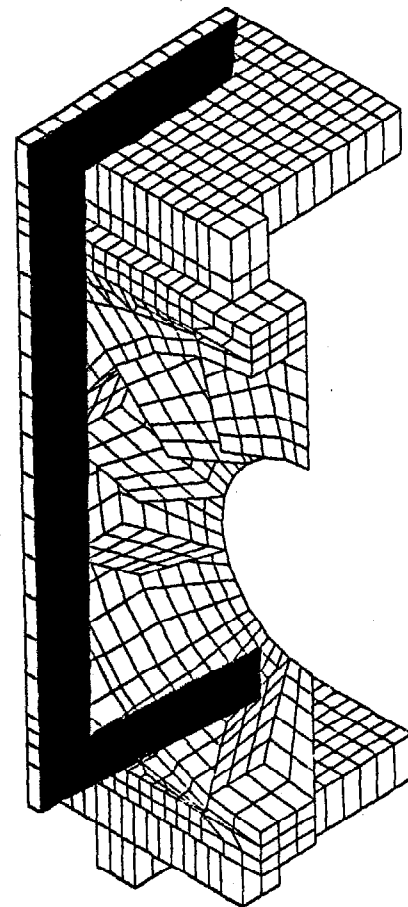
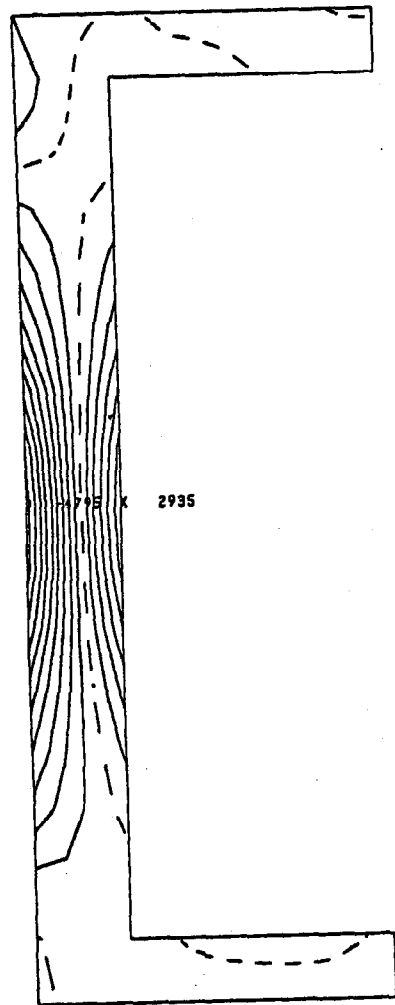
Fig. 10 Beam Model of Lower Return Leg with "Roman Arch Loading"



COMBINED LOADING

Fig. 11 Von Mises Effective Stress in Ring and Frame for Combined Operational Loading

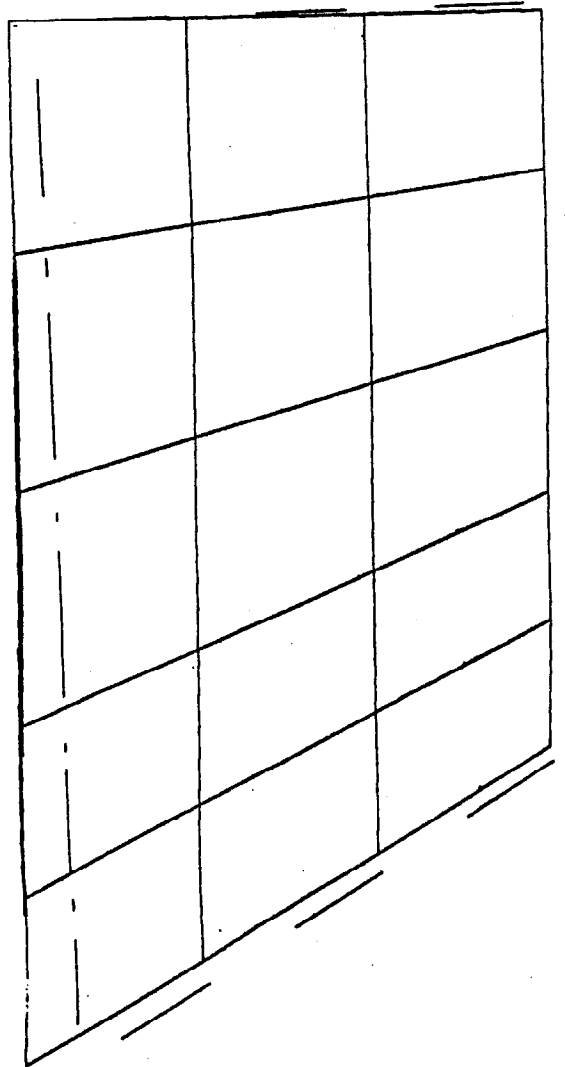
STEP= 1 ITER= 1 TIME=



COMBINED LOADING

Fig. 12 Bending Stress Contours for Combined Operational Loading

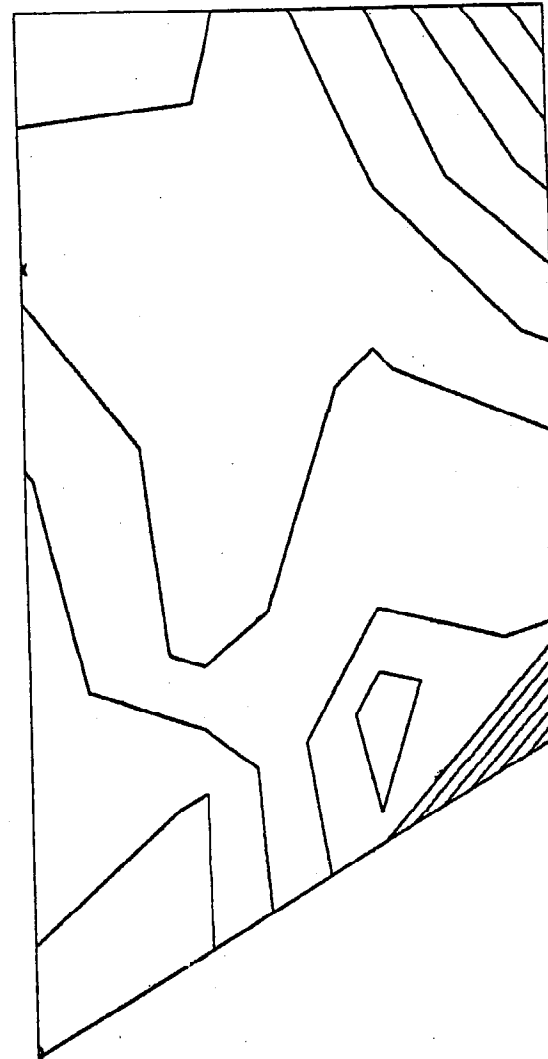
STEP= 1 ITER= 1 TIME= 0



TYPICAL RIB-COMBINED LOADING

(a)

STEP= 1 ITER= 1 TIME= 0

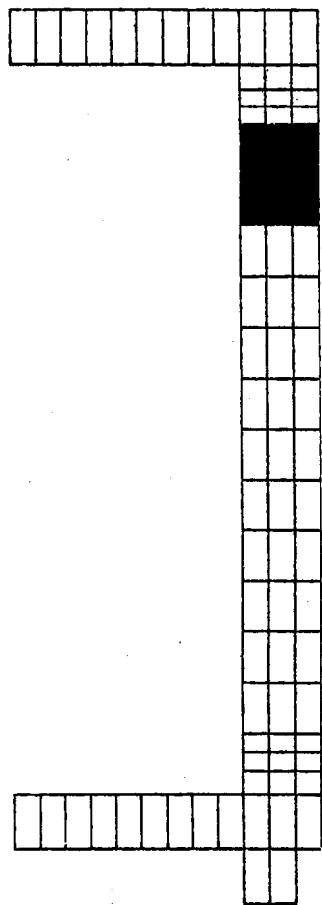
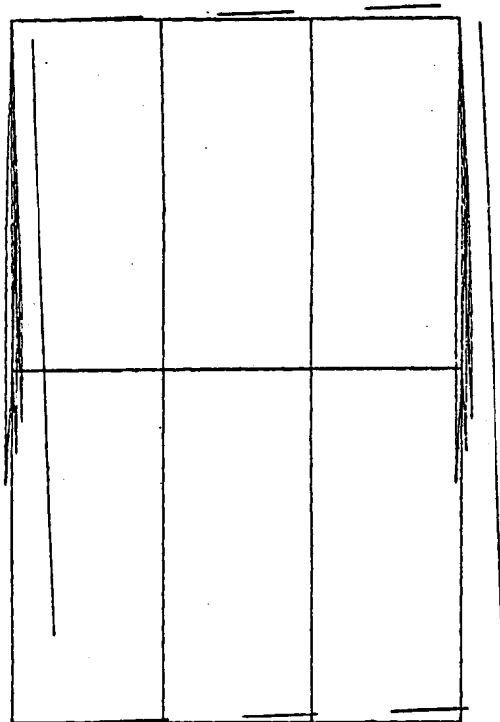


TYPICAL RIB-COMBINED LOADING

(b)

Fig. 13 Deformation and Von Mises Effective Stress Contours in Typical Rib for Combined Operational Loading

STEP= 1 ITER= 1 TIME= 0



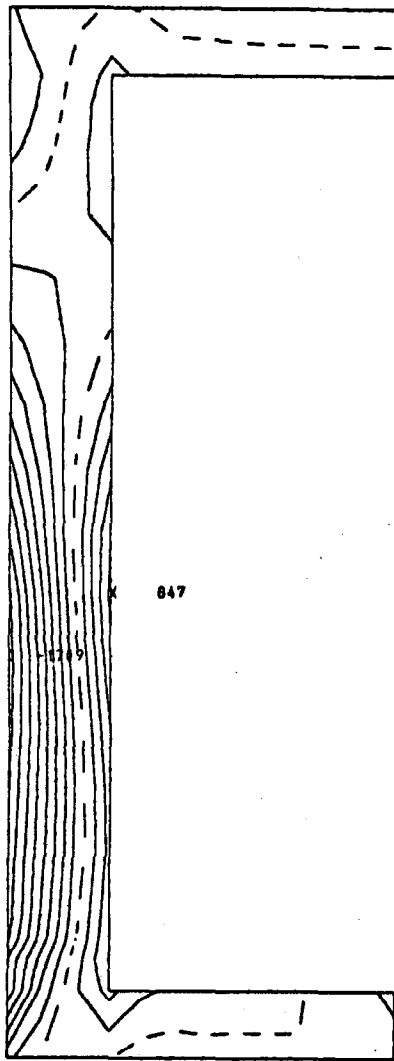
(Stresses are in element coordinate system shown)

| | | |
|-------------------|-------------------|-------------------|
| $\sigma_x = -95$ | $\sigma_x = -4$ | $\sigma_x = 105$ |
| $\sigma_y = -83$ | $\sigma_y = 197$ | $\sigma_y = 366$ |
| $\tau_{xy} = 303$ | $\tau_{xy} = 368$ | $\tau_{xy} = 359$ |
| $\sigma_x = 16$ | $\sigma_x = 58$ | $\sigma_x = 60$ |
| $\sigma_y = -11$ | $\sigma_y = 301$ | $\sigma_y = 543$ |
| $\tau_{xy} = 493$ | $\tau_{xy} = 520$ | $\tau_{xy} = 636$ |

MAIN DIAGONAL-COMBINED LOADING

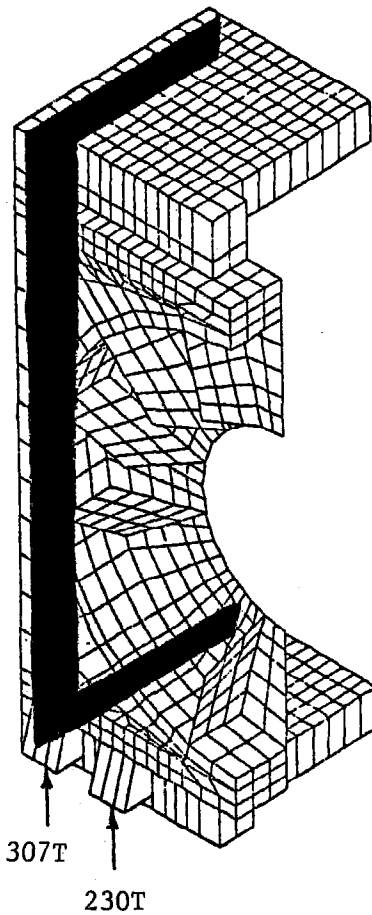
Fig. 14 Deformation and Centroidal Stresses in Main Diagonal (psi)

STEP= 1 ITER= 1 TIME= 0



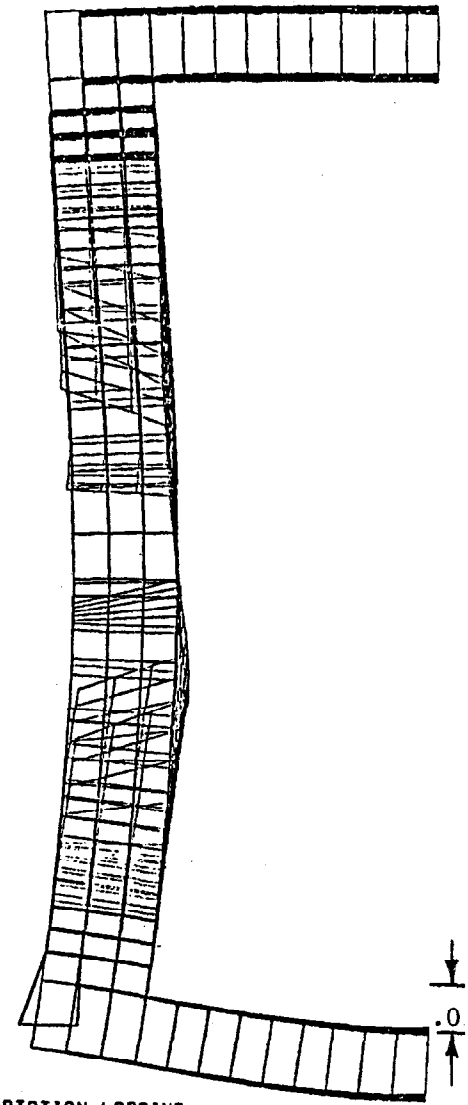
TRANSPORTATION LOADING

(c) Bending Stresses in Legs and Frame



(b) Reaction Forces at Supports

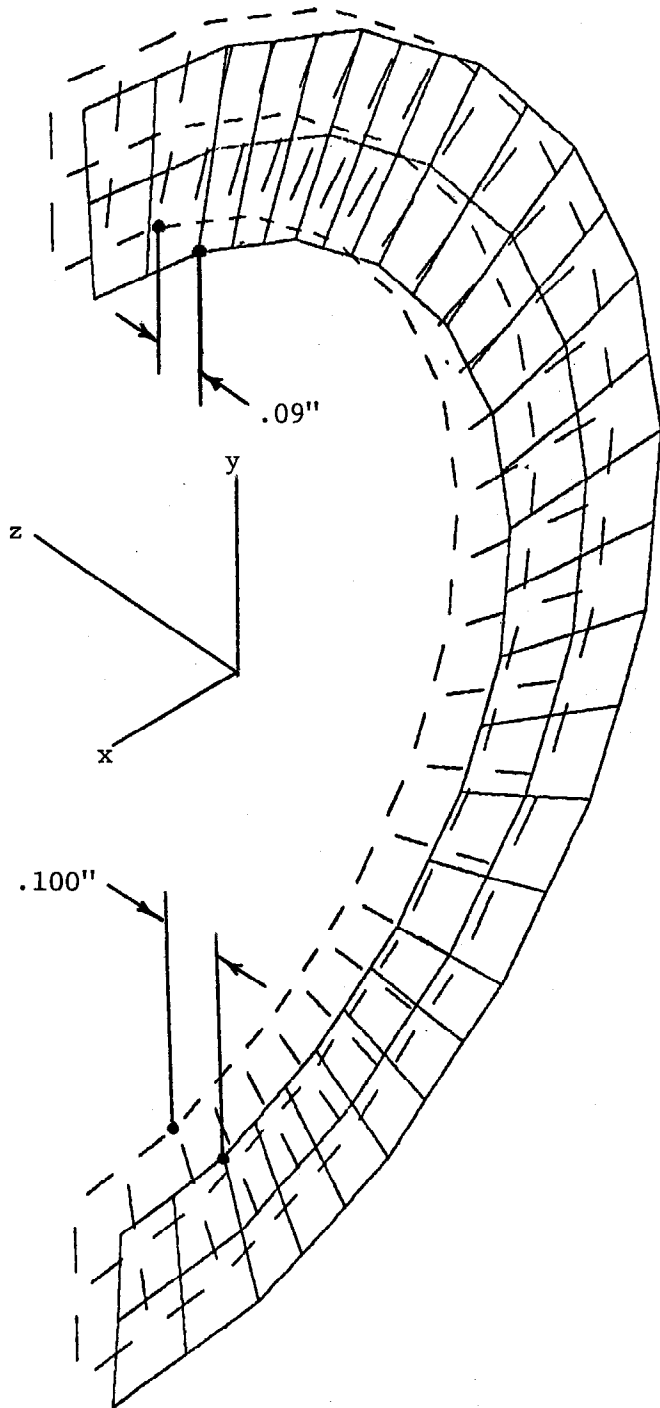
STEP 1 ITER 1 TIME .00



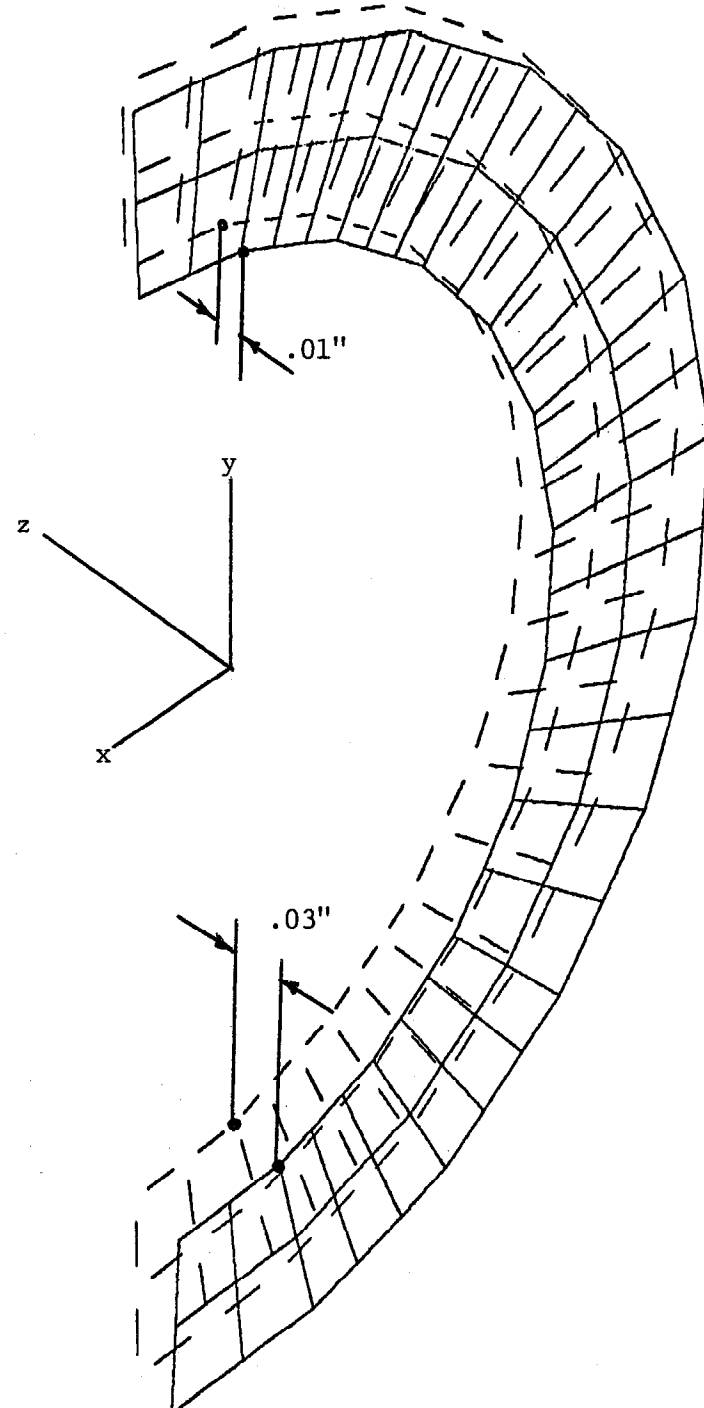
TRANSPORTATION LOADING

(a) Distortion of Legs and Frame

Fig. 15 Transportation Loading

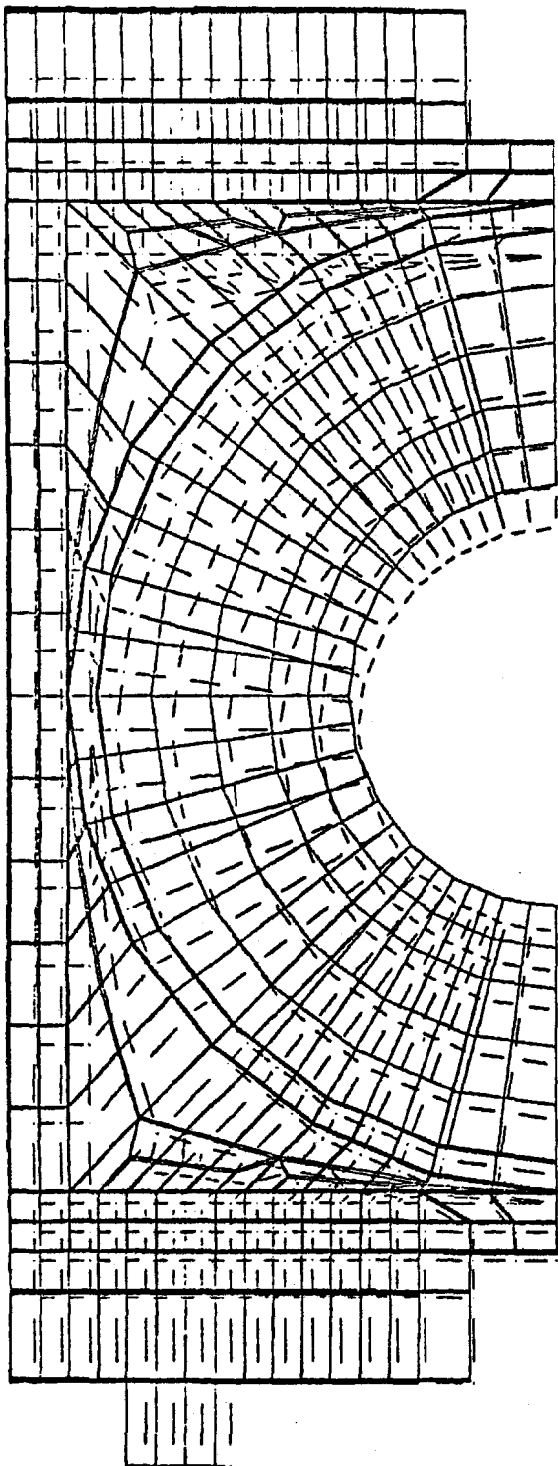


DEFORMATION IN ANNULAR PLATE UNDER COMBINED OPERATIONAL LOAD
(a)



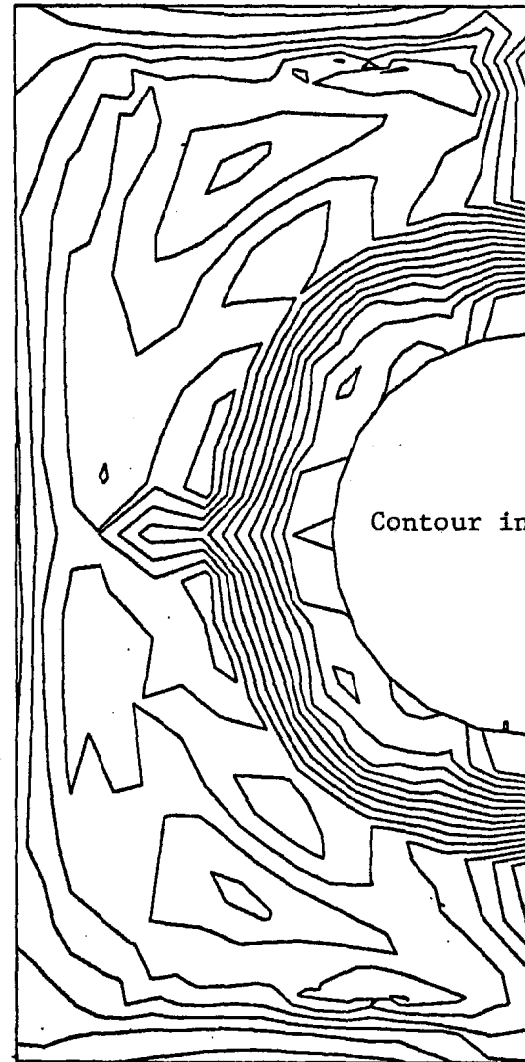
DEFORMATION IN ANNULAR PLATE UNDER TRANSPORTATIONAL LOAD
(b)

Fig. 16



(a) Distortion offrams

STEP= 1 ITER= 1 TIME= 0



Contour interval = 250 p

YOKESA THERMAL LOAD

(b) Von Mises Effective Stress Contours at Carbon Steel/Stainless Steel Interface

Fig. 17 Thermal Loading

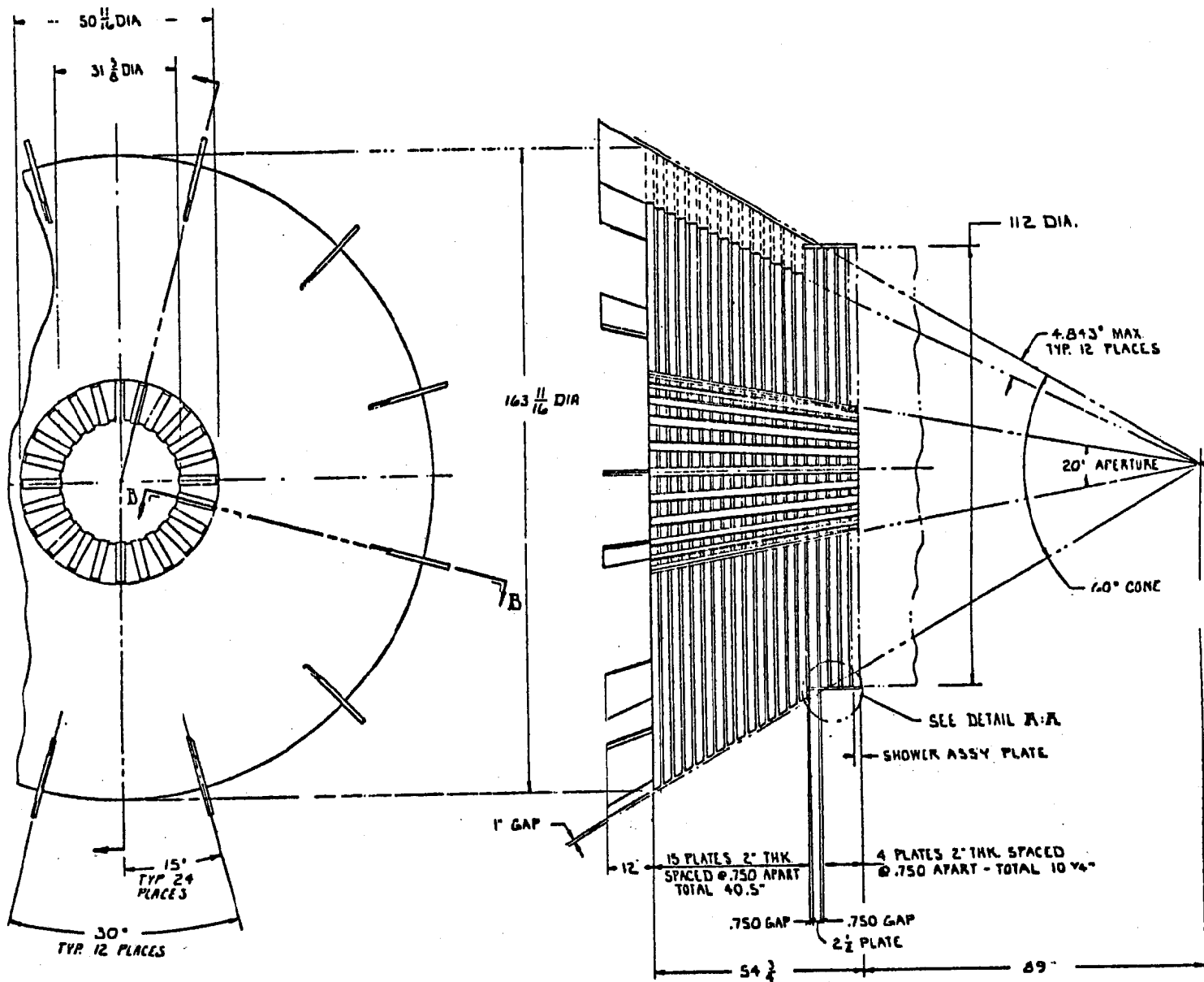


Fig. 18. Endplug as Analyzed

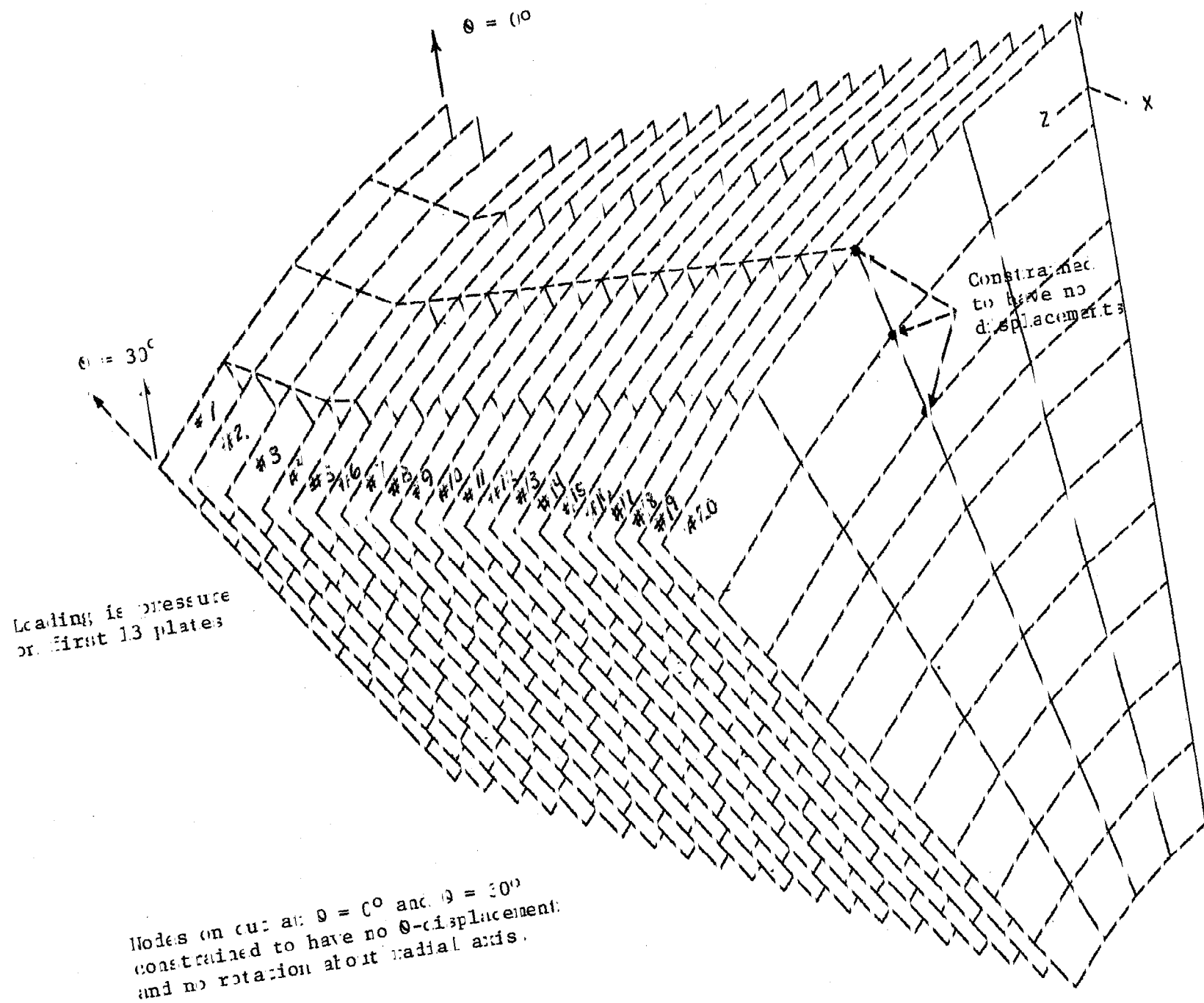


Fig. 19 Crucé Plug Model

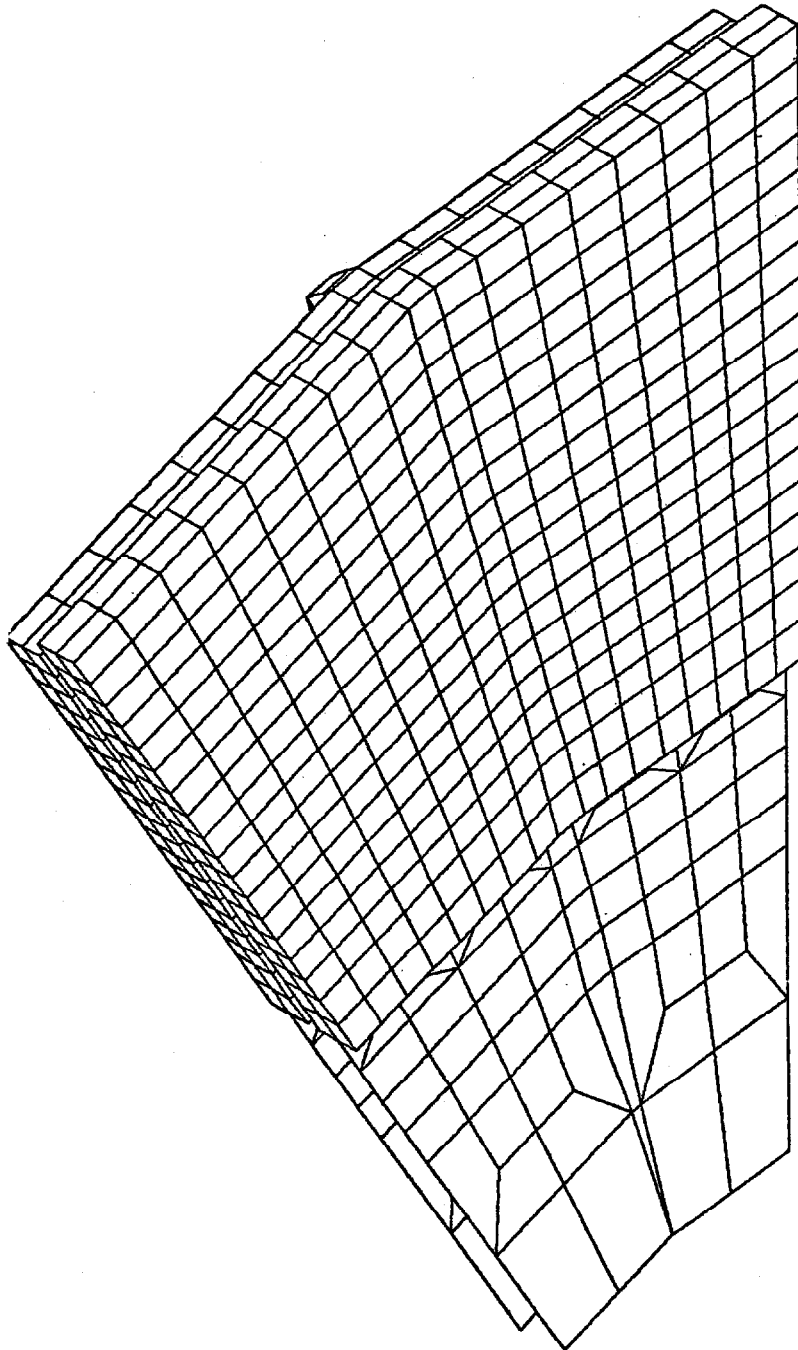


Fig. 20 Refined Plug Model

STEP 1 ITER 1 TIME .00

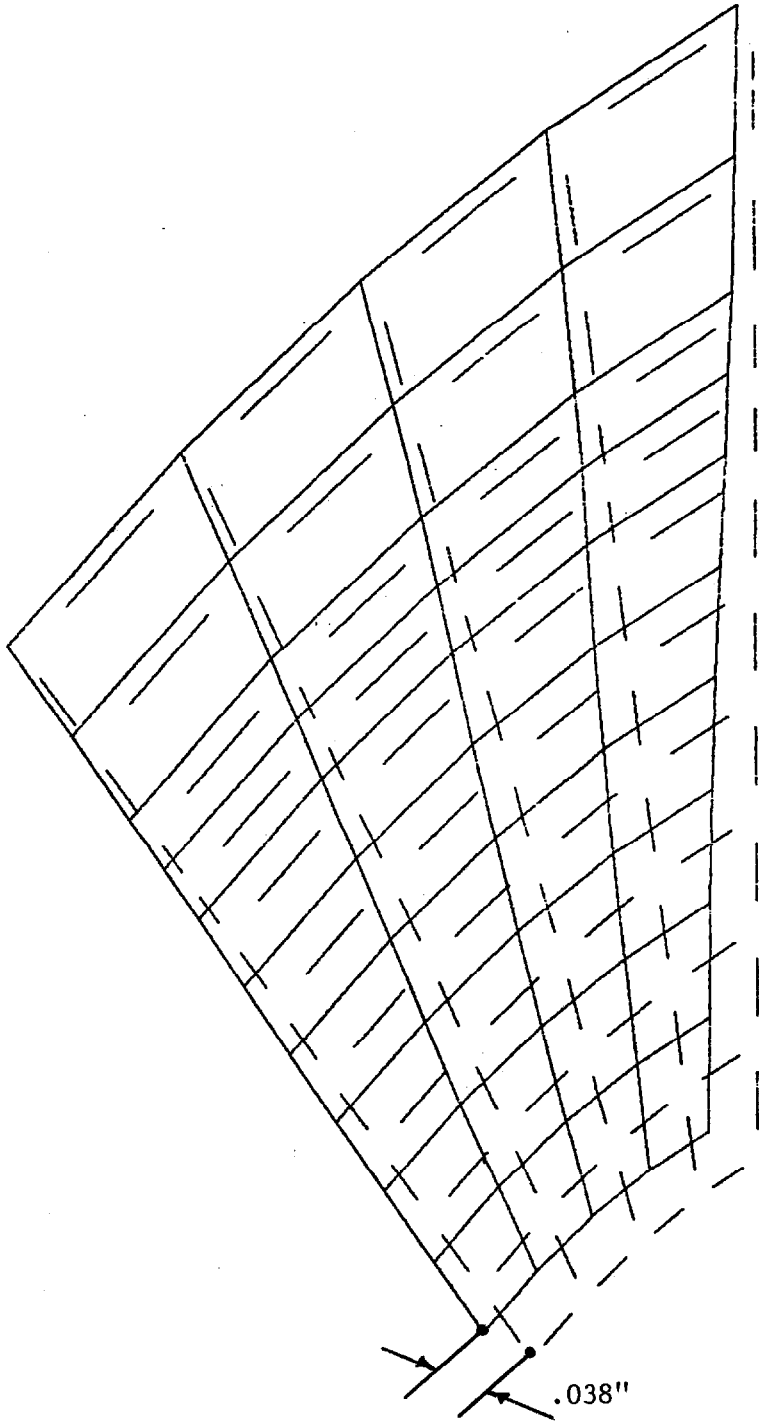


PLATE NUMBER 7

Fig. 21 Deformation in Plate 7 in Crude Plug Model

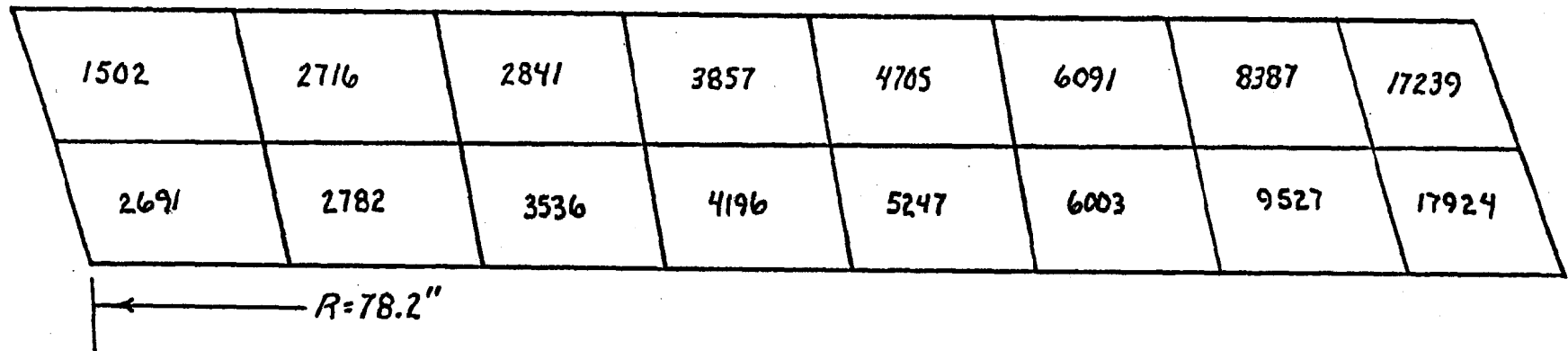
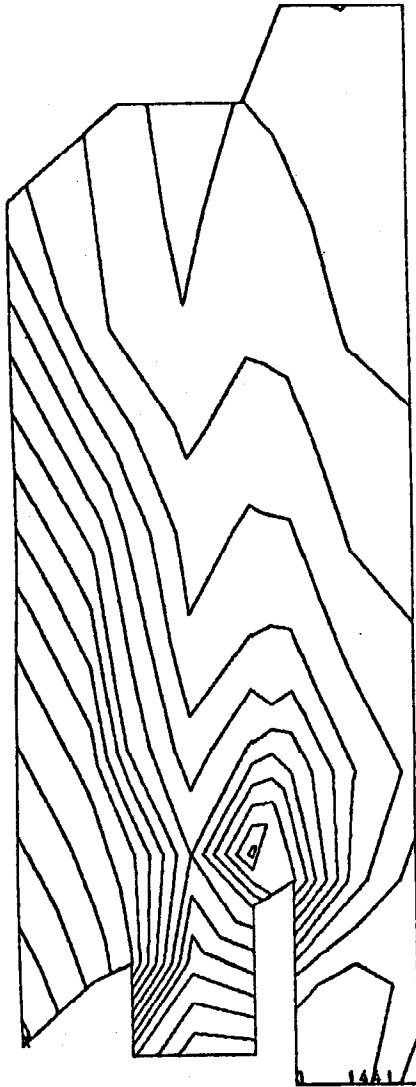


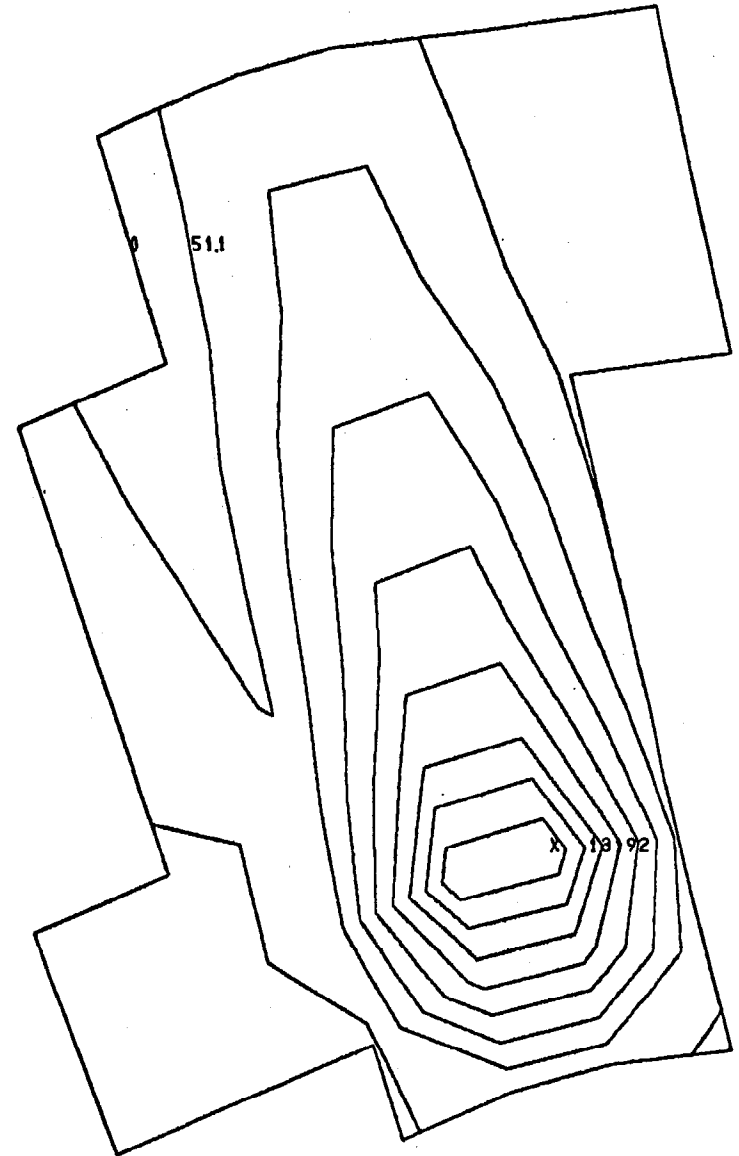
Fig. 22 Von Mises Effective Stress at Centroids of Elements in Rib Between Plates 19 and 20 (psi)

Section is taken halfway through rib.
Contour interval = 1500 psi.



REFINED PLUG SOLUTION RUN-1.5 INCH RIB
(a)

Section is taken just below rib in
Plate 19. Contour interval = 1500 psi



REFINED PLUG SOLUTION RUN-1.5 INCH RIB
(b)

Fig. 23 Von Mises Effective Stress Contours in Section of Rib between Plates 19 and 20